Theoretical and Experimental Modal Analysis of a 6 PUS PKM

Francesco La Mura[1][a], Hermes Giberti[1][b], Linda Pirovano[2] and Marco Tarabini[2]

[1]*Universita' degli Studi di Pavia, Dipartimento di Ingegneria Industriale e dell'Informazione,*
Via A.Ferrata 5, 27100 Pavia, Italy
[2]*Politecnico di Milano, Department of Mechanical Engineering, 20156 Milano, Italy*

Keywords: Modal Analysis, Parallel Kinematics Machines, Multibody, Natural Frequencies.

Abstract: In this article the modal analysis of a manipulator is presented and discussed from a theoretical and experimental perspective. The work focuses on both the simulation and the experimental stages of the modal analysis on six DOF parallel kinematics machine. In particular, the behavioural vibrational trend of the kinematics structure under analysis is presented within the entire workspace. Critical aspects of each test phase are highlighted as well as data post processing methods used. Finally, a map capable of summarizing the modal analysis results is shown.

1 INTRODUCTION

Differing poses of a manipulator within the workspace can show completely different behaviour in terms of natural frequencies that could cause serious vibrations and consequently instability in the movement of the end effector, reducing accuracy (Mejri et al., 2016; Wiens and Hardage, 2006; Silvestri et al., 2011; Confalonieri et al., 2018). This aspect must be taken into consideration when one is dealing with the design of a new robotic device and in particular in the case of a parallel kinematic architecture where the highly non linear kinematics and the difficulty in realising joints and kinematic constraints make the a priori evaluation of this problem extremely difficult to assess.

In this work a procedure used for the modal characterisation of a 6 DOF PKM for HIL testing is presented and analysed in depth. This device, called Hexafloat, was designed and realised within the ambit of the H2020, LIFES50+ project at the Politecnico di Milano (Bayati et al., 2014; Giberti et al., 2018). By using this robot one can move a scaled model of a wind turbine within the wind tunnel, simulating a floating wind generator moving in a deep sea environment (Bayati et al., 2017; Giberti and Ferrari, 2015).

The Robot target position and orientation are calculated in real-time resolving floater dynamics within a force loop(La Mura et al., 2018b). This aspect joined to the high inertia of the scaled wind turbine, its flexibility and the required dynamics bandwidth of

the floater must be taken into account carefully in order to obtain a good transparency behaviour (La Mura et al., 2018a) of the HIL device. In order to obtain these results, it is useful to identify the Hexafloat natural frequencies. This analysis can be limited to the manipulator first natural frequency. The main goal is to verify that the robot has its first natural frequency well above both the range exploited by the floater motion $(0 - 3hz)$, and the first frequencies of the turbine being tested. For this type of study simulated and experimental analysis must be conducted together in order to interpret the results correctly and support the definition of the experimental setup.
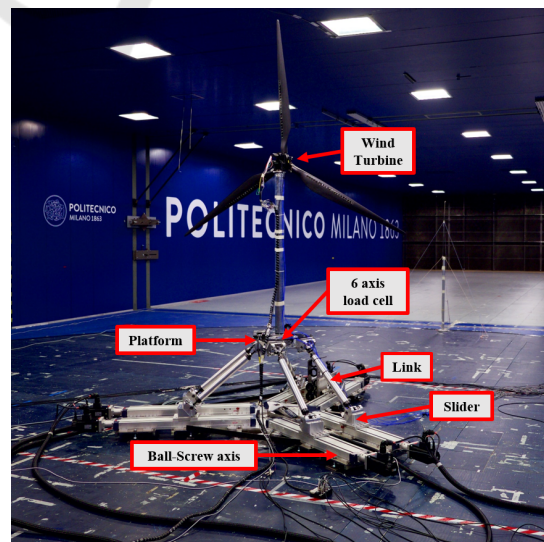

Figure 1: Hexafloat robot main components.

[a] https://orcid.org/0000-0001-5143-7120
[b] https://orcid.org/0000-0001-8840-8497

2 MULTIBODY MODEL

Hexafloat PKM architecture, shown in the figure 1 is made up of three main components: a platform, carrying the turbine and load sensors; six identical legs each belonging to a different kinematic chain; six actuation chains made up of a translating carriage, a joint holder, a lead screw and a brushless motor directly connected to it.

The objectives of the analysis described in this paper are, for all possible configurations of the robot within its workspace to evaluate modal shapes and their variation in different poses and to define the configurations corresponding to absolute and local minima of the first natural frequency.

In order to meet these objectives, the Hexafloat model is developed with Adams®, a multibody software able to reproduce robot dynamics and to perform a vibration study, choosing between rigid and flexible behaviour among different components. Therefore, few components have been neglected or simplified in order to reduce computational cost taking into account major components influences.

The platform is modelled as a rigid body due to its specifically designed shape, compact dimensions, high performance materials that bring to orders of magnitude lower deformations compared to the link ones.

Links model are made of three flexible bodies: at the far end of the link, two elements made of steel perfectly reproduce the geometry, dimensions and mass parameters of the connecting rod, bearing case and distance washer while in the middle an aluminium hole cylinder stands for the main leg component. Sliders are a simplification of joints located at the basis and they replicate the behaviour of a translating mass.

Moreover, the robot model is completely parametrized and created through the use of Adams®MACRO.

This approach, combined with Co-Simulation between Matlab and Adams®, is able to efficiently explore all different configuration needed.

Stiffness, dumping and load transfer to actuators change widely depending on the configuration assumed. Natural frequencies evaluation is performed investigating a grid of positions assumed by the Hexafloat TCP on three different planes fig. 2.

That are defined considering a rotation of an angle ϕ around the z global axis. The angle ϕ covers three different values: $0°, 45°$ and $90°$. The first plane with $\phi = 0°$ correspond to global Y-Z plane, while the last one, $\phi = 90°$, identifies global X-Z plane. On each plane discretization steps are defined, of 25mm along Z and Y axes and 50mm along X-
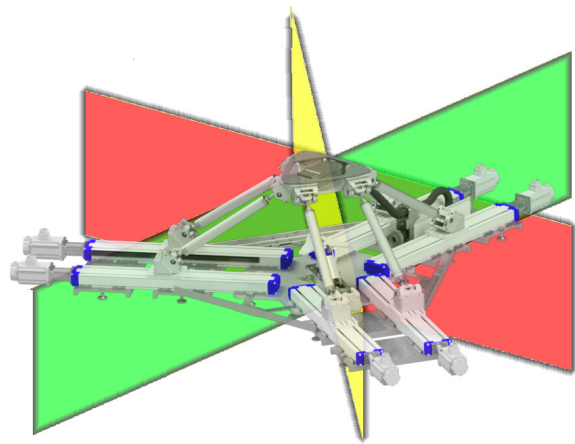

Figure 2: Testing points for the simulation.

axis, as shown in fig. 2. The grid points are defined in order to have always 7 points along each plane axis, thus a total of 49 points in each plane. Lower and upper bounds for both X, Y and Z are given by nominal workspace dimensions of $[\pm150, \pm75, \pm75]$ mm, around nominal Home Position (with null orientation and position coordinates $[0, 0, 463.6]$). The platform orientation is described by a set of three cardanic angles, called roll, pitch and yaw (α, β, γ), respectively as a rotation around X-axis, Y-axis and Z-axis. With the following values: Roll α $-5°, 0°, 5°$; Pitch β: $-8°, -4°, 0°, 4°, 8°$ and Yaw γ: $-3°, 0°, 3°$.

The natural frequencies evaluation was performed for all the possible combinations of these three angles with an iterative procedure: for each position in the grid, the Adams®MACRO routine is run and a new model is created for every possible orientation. Given 45 different angular configurations for each point, a total of 2205 combinations are tested on every plane. In each point a static equilibrium is imposed and the first eigenfrequency is evaluated.

3 SIMULATION RESULTS AND DISCUSSION

Trends results on $\phi = 0°$ plane are shown in fig. 3. Each coloured plane identifies a fixed orientation configuration. The resulting surfaces show the variation of the first frequency while moving inside the $\phi = 0°$ plane, thus changing Y-Z value on the grid. The overall trend is most of the time a paraboloid, with a maximum value for DOF combination corresponding to robot best and stiffest attitude. Frequency mean value, standard deviation and percentage maximum variation are computed as well. All this statistical descriptors are reported in tab. 1.
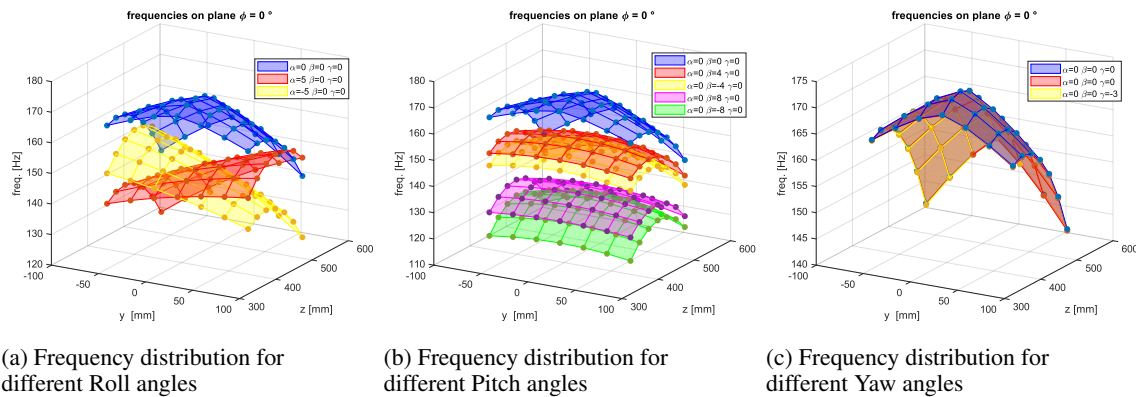
(a) Frequency distribution for different Roll angles

(b) Frequency distribution for different Pitch angles

(c) Frequency distribution for different Yaw angles

Figure 3: Frequency distributions on $\phi = 0°$ plane (Y-Z).

Table 1: Results summary on the plane $0°$.

Angle		Min[Hz]	Max[Hz]	Mean[Hz]	Std[Hz]	Max.Δf[%]
	$0°$	143.67	171.25	161.71	6.79	16.11
α	$5°$	123.73	155.49	144.15	7.07	16.61
	$-5°$	123.64	155.29	144.00	7.04	16.58
	$0°$	143.67	171.25	161.71	6.79	16.11
	$4°$	137.75	154.42	149.28	4.27	10.73
β	$-4°$	134.21	151.87	146.13	4.24	11.63
	$8°$	122.28	134.35	129.69	3.42	8.98
	$-8°$	116.26	129.87	124.29	4.00	10.39
	$0°$	143.67	171.25	161.71	6.78	16.11
γ	$3°$	143.37	171.14	161.58	6.80	16.23
	$-3°$	143.51	171.14	161.58	6.80	16.14

Roll Angle Influence: as shown in fig. 3a, for positive Roll rotations, maximum frequencies are registered along positive Y-axis direction while for negative rotations maxima are located along negative Y-axis direction, showing a symmetric distribution as expected. Z variation reveal an optimum height on which first frequency have a local maximum and whose value change with Y and angle combinations. Absolute highest and lowest frequencies are registered at Y boundaries. Angular rotations of the same sign of the Y displacement lessen the machine asymmetry and so the manipulator assumes a more structurally rigid position, thus enhancing 1st natural frequency value.

Pitch Angle Influence: by varying the Pitch angle, frequency distribution exhibits changes as well. The same trend is preserved for every angle value, except for mean value that decreases as the angle increases its magnitude. This behaviour is clearly shown in fig. 3b. The lowest frequencies are registered for $\beta = -8°$ for which Hexafloat legs are in the most asymmetric configuration. Negative rotations induces always a larger frequency reduction with respect to positive rotation of the same magnitude, this is due to

different number of legs approaching singular configuration. Greater influence of Pitch angle is near the centre of the Y-Z plane while at the boundaries, the frequency decreases due to the already high asymmetry of the legs arrangement caused by Y and Z variation.

Yaw Angle Influence: the frequency distribution is not affected by a variation of Yaw angle as shown in fig. 3c, as only differences caused by non zero Y and Z coordinates arise.

The same analysis was performed for $\phi = 90°$ and $\phi = 45°$. For the sake of brevity the results are not reported.

4 EXPERIMENTAL MODAL ANALYSIS

Experimental modal analysis is based on the measurements of structure FRFs. This measurement requires an excitation in one or more locations and collection of vibratory response in multiple positions (Fu and He, 2001). In many experimental investigation regarding manipulators natural frequencies (Palmieri
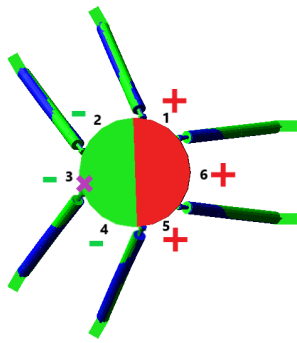
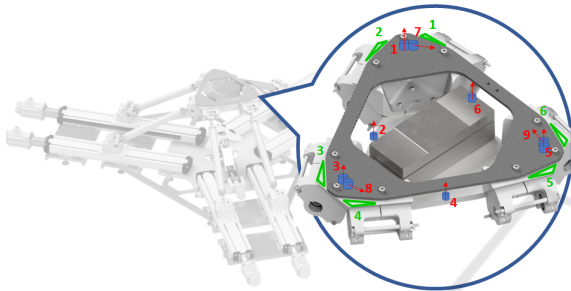Figure 4: First vibration mode: vertical displacement sign of the tilting platform.

Figure 5: Accelerometers location (blue), measuring direction (red) and hitting points (green).

et al., 2014; Vu et al., 2016), the entire structure is scanned by placing sensors onto each structural element.

By means of the modal shapes tracking obtained by the simulation, sensors number and placement was chosen effectively, avoiding uselessly expensive and burdensome setup and data post processing. As shown in fig.4, being the first and second mode characterised by a clear platform tilt, namely a rigid rotation, each platform point not located on the rotation axis, have an acceleration component in Z direction. The rotation axis virtually cut the platform in two section, each of which has homogeneous Z acceleration sign (fig.4). Analysing the reciprocal phase between accelerometers and input force, modal shapes can be then re-identified from experimental data.

Six accelerometers are located onto the platform: one placed onto each joint block and the other three arranged on the platform in between of each legs couple. The described arrangement allows to have at least 2 sensors detecting one of the two coupled frequencies. For a robust mode identification, also accelerometers not measuring along Z direction are required. Three more sensors are positioned onto the platform (7,8 and 9 in fig. 5), each one onto a joint block, measuring in the direction tangent to the circle enclosing the platform joints.
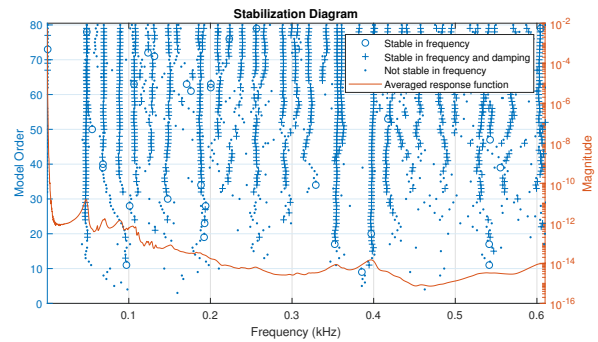

Figure 6: Stability diagram obtained with multiple LSCE analysis.

4.1 Experimental Procedure

The procedure adopted during the experimental tests is briefly summarized as follows. Hexafloat is moved in the i-th testing pose. The impact hammer hits the structure in the first hitting location for the i-th pose and the response is acquired for at least 5*s*. This operation is repeated 5 times. The impact hammer hits the structure in the second hitting location for the i-th pose and the response is acquired for at least 5*s*. This operation is repeated 5 times. Orientation is changed and points 2 and 3 are repeated until all possible angle combination are covered. After that, point 1 is repeated and another grid point on the plane is explored. This procedure is repeated on each chosen plane. Impact points are chosen by observing simulated modal shapes changing detected and avoiding vibratory nods while maximizing expected vertical acceleration lecture.

4.2 Measurements Setup

Measurement chain components are briefly summarized hereafter. **Impact hammer:** PCB[®] 086C03 model with a 2.25 mV/N sensitivity. The hammer is equipped with a medium hardness plastic tip and a extender mass weight of 75 grams with the aim of introducing a suitable amount of energy able to excite the structure over a wide frequency range. **Piezoelectric accelerometers:** Bruel&Kjaer[®] 4508 model has high sensitivity, low mass and small physical dimensions that make this sensor suitable for modal investigation in rough environments. They have a frequency range of 0.4–6000*Hz*, a 10 mV/ms^{-2} sensitivity and a mass of 4.8 grams. **DAQ system:** NI[®] Compact-DAQ-9178 with 8 slots in which C-Series I/O module are plugged in. Three NI[®] 9402 C-series I/O module equipped with 4 bidirectional channels with BNC connectivity and a 55*ns* update rate are employed. Signals are acquired by mean of Politecnico di Milano

MeasLab software. The signals are acquired with a sampling rate of 2048 Hz and each test has a duration of 5*s*, thus ensuring a frequency resolution of 0.2 Hz.

5 DATA POST-PROCESSING METHODS

Natural frequencies extrapolation from system Frequency Response Functions (FRFs) is a key step in data post-processing. This operation is done by checking FRFs plot and using other methods such as Least-Square-Complex-Exponential (LSCE). This method requires the computation on impulse response function associated to each FRF. Each impulse response is expressed by a series of complex damped sinusoids, in the form of exponential functions, which contain eigenvalues and eigenvectors (Brandt, 2011; Allemang et al., 1994).

The LSCE method allows one to individuate the system natural frequencies through system poles extraction. The number of poles considered in the analysis is really affecting the obtained results. To overcome this limitation, the identification is carried out for increasing model orders. As the model order is increased, more and more modal frequencies are estimated but the estimates of the physical modal parameters will stabilize as the correct model order is found (Allemang et al., 1994). Physical modes are easily distinguish from spurious modes related to noise or other computational issue: the first ones constantly arise for different model order while the second ones randomly appears. A straightforward example is reported in fig. 6. The vertical straight lines in fig. 6 show up in correspondence of natural frequencies, but only the ones characterised by vertical lines both stable in frequency and damping can be trusted. The natural frequency extraction is done for all the measured data in all the tested Hexafloat poses by mean of the natural frequencies evaluation from stability diagram of the averaged FRFs measured in each pose. The doubly stable obtained values are compared with the ones in FRFs magnitude and phase plots to confirm the results. Figure 7 demonstrates the goodness of both results obtained with stability diagram and the ones reported in FRF plot for the $\{-150, 0, 538.6, 0°, -8°, 0°\}$ configuration. Useful methods adopted for coupled modes are *Single Value Decomposition*(SVD) and *Complex Mode Indicator Function*(CMIF), not described here for brevity.
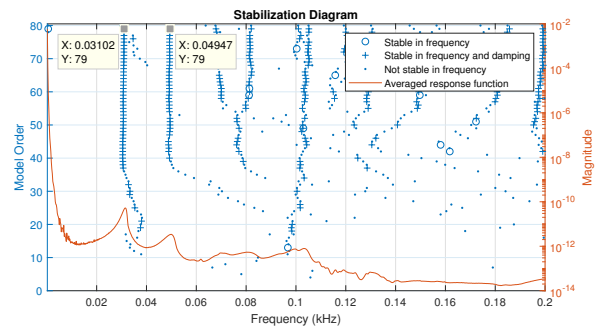
(a) Stability diagram
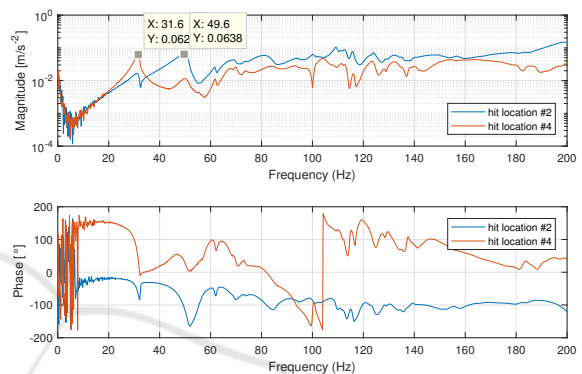
(b) Acelerometer #1 FRF

Figure 7: 1st and 2nd natural frequencies in $\{-150, 0, 538.6, 0°, -8°, 0°\}$ configuration.

6 EXPERIMENTAL RESULTS

Due to the mathematical model approximation, the 1st natural frequencies is lower compare to the simulated one: taking into consideration the *Home Position* configuration with null angular orientation, 47 Hz is the experimental value compared to 170 Hz the one simulated. This difference is due to model approximations, such as passive joints considered ideal and rigid, as well as the fixed base.

Despite this difference and according to the objectives of the work, simulations and experimental results succeed in minimum frequency configuration identification, first mode trends evaluation and mode shapes re-construction.

The first resonance peak is at a very low frequency and it exhibits a clear 180° phase change, thus revealing the presence of a physical mode of vibration. This resonance peak shows up in all accelerometers FRFs at almost the same frequency value in both two hitting points. An example is provided in fig. 8, in which the platform is hit in location #4, indicated with violet cross, while numbers identify sensors location. Looking at the sign of the phase diagram (fig. 8b), the plat-

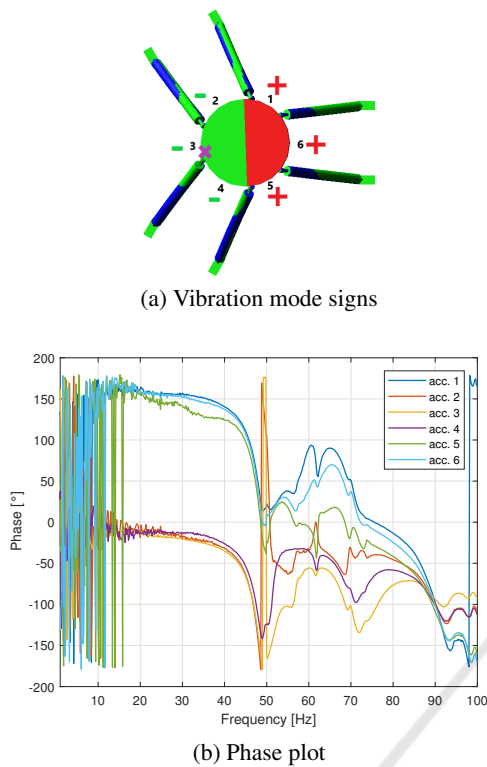(a) Vibration mode signs

(b) Phase plot

Figure 8: Vibration sign check.

form exhibits a vibration similar to the one resulting from simulation: half of the platform vibrate in phase with the hammer hit while the other one in counter phase

Additional peaks appear at a frequency around 60 Hz. This multiple peaks does not correspond to a clear phase shift, thus revealing the possibility of being induced by few other symmetric components that does not mainly vibrate in the investigate direction. A prominent peak characterised by a clear phase shift emerges around 80 Hz. Analysing in detail the sign of the phase plot for all the accelerometers, it can be stated the vibration is always in phase with the hit direction, thus highlighting a prominent movement along z-direction with no relevant rotation and so discarding this one from the simulated 1st mode of vibration search.

Verification of mode decoupling is also required. The FRFs computed from different hits should be characterised by not all the accelerometers reading the same first frequency value, being some of them in nodes for one of the two no more coupled modes. The above mentioned requirements can be found in fig. 7b and 9. For the sake of brevity, only the $\{-150, 0, 538.6, 0°, -8°, 0°\}$ pose configuration is reported even though the correct simulated behaviour is found for all the experimentally tested poses. From
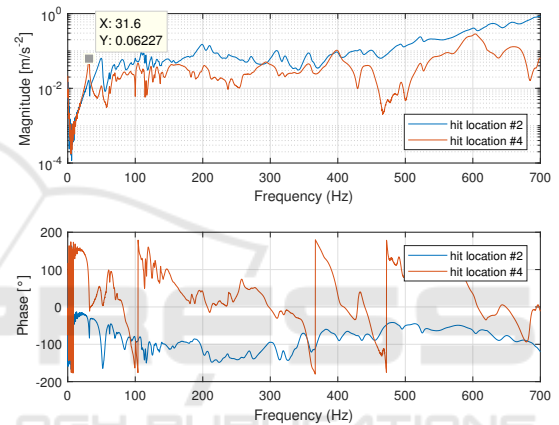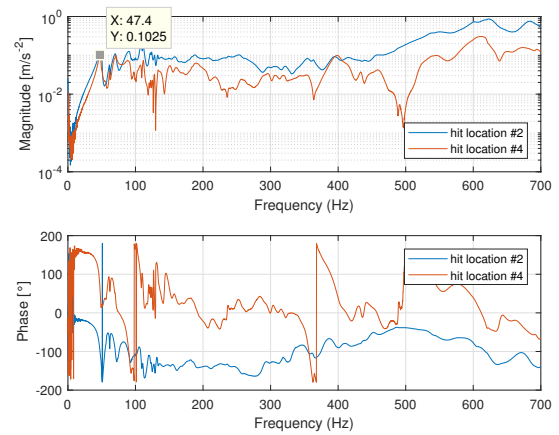

(a) *Home position*

(b) $\{-150, 0, 538.6, 0°, -8°, 0°\}$ configuration

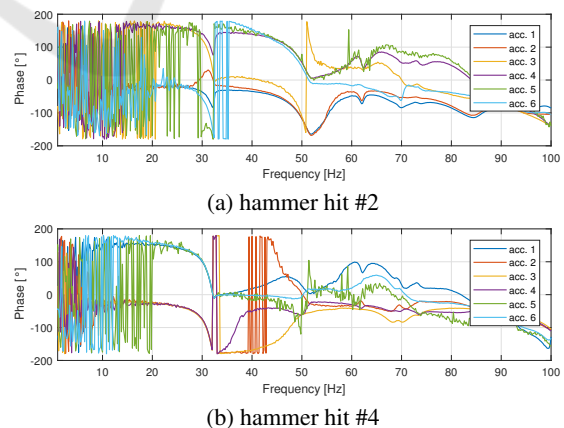Figure 9: Accelerometer #1 FRF.

(a) hammer hit #2

(b) hammer hit #4

Figure 10: Phase diagram of FRF in $\{-150, 0, 538.6, 0°, -8°, 0°\}$ configuration, zoom on [0:100]hz.

47 Hz in *Home Position*, peak value moves to 31 Hz, accordingly with simulated reduction (98 Hz vs. the

Home Position 170 Hz). A new peak appear at 49 Hz, not present in the *Home Position*, validating the decoupling of the two modes due to the asymmetry of the manipulator structure in this pose (fig. 7b).

Once correspondence between experimentally identified modes and simulated one has been assessed, it is possible to compare frequency shift trends. Since absolute frequency values do not correspond, the comparison is done normalizing all the frequency values with respect to results in maximum Z and null X, Y. Instead, when examining angle variation influence, a different normalization is adopted: data are normalized with respect to the null angle configuration, referring to the value associated to $x = 0$ in $90°$ plane or $y = 0$ in $0°$ plane.

Translation Effect on Y-Z Plane: the frequency distribution in $0°$ plane has the expected parabolic trend (fig. 11). Experimental data confirm the symmetric data distribution obtained in simulations. The behaviour of normalized data as z-coordinate decreases is confirmed as an increase in frequency is correctly detected.
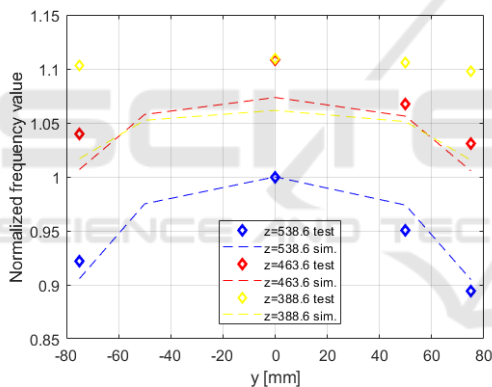

Figure 11: $0°$ plane frequency trend.

Translation Effect on X-Z Plane: both simulated and experimental frequency trends on $90°$ plane for different z values are characterised by a parabolic shape (fig. 12). Z-coordinate effect appears stronger on experimental results at workspace boundary regions.

Roll Influence on X-Z Plane: a good correspondence in terms of frequency trend can be extrapolate from X-Z plane (fig 13), in which the parabolic distribution shows up for both experimental and simulated results. As expected, positive and negative Roll angles does not causes a significant frequency difference. Experimental results shown higher normalized frequencies compared to the normalized simulated results, thus revealing slightly less sensibility to pose change.

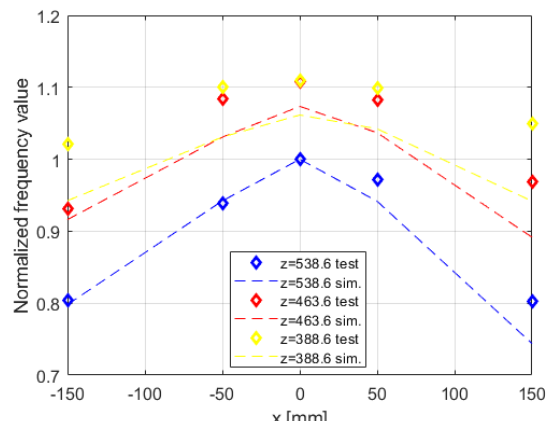**Pitch Influence on Y-Z Plane:** fig. 14 illustrates

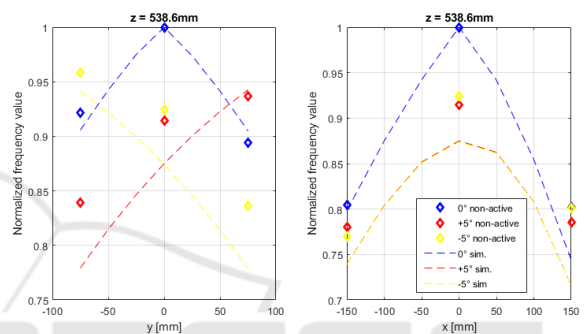Figure 12: $90°$ plane frequency trend.

Figure 13: Roll angle influence.

frequency distribution caused by Pitch angles. Normalized frequency values obtained from experiments are greater with respect to the ones computed in Adams®. Anyhow the distribution trend is correctly reproduced.
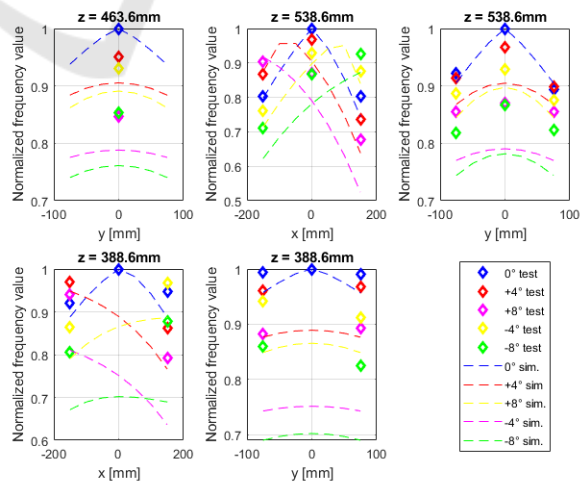

Figure 14: Pitch angle influence.

Yaw Influence: as expected from the simulation, experimental Yaw angle variations can be consid-

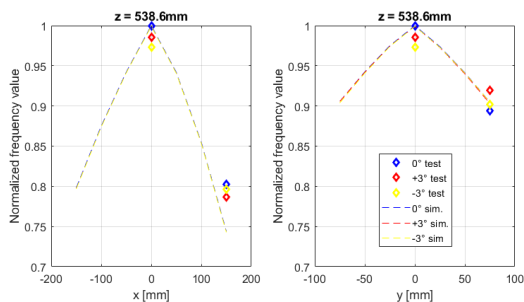ered negligible in the frequencies distribution into workspace (fig. 15).

Figure 15: Yaw angle influence.

7 CONCLUSIONS

In this article, a complete methodology for modal analysis of a 6 DOF parallel kinematics robot is proposed. In alternative to literature methods, the proposed procedure do not use complex simulations setup and expensive experimental campaigns. Simulation analysis has been designed in order to be simple and effective, with the only support of a approximate flexible-multibody model. Simulation campaign has highlighted: modal shapes and their change through workspace exploration, sensor and hitting points optimum configuration and minimum first frequency robot configuration. These information has been used for optimal experimental campaign design and identification of a small set of configuration on which fine FEM simulation could be set up. Experimental campaign has been setup with minimum amount of sensors and effective testing procedure. A complete data post processing method has been also proposed, particularly suitable con complex PKM with coupled modes and taking into account real world data issues.

REFERENCES

Allemang, R. J., Brown, D. L., and Fladung, W. (1994). Modal parameter estimation: a unified matrix polynomial approach. In *Proceedings - SPIE The International Society For Optical Engineering*, pages 501–501. SPIE Internation Society For Optical.

Bayati, I., Belloli, M., Bernini, L., Giberti, H., and Zasso, A. (2017). Scale model technology for floating offshore wind turbines. *IET Renewable Power Generation*, 11(9):1120–1126.

Bayati, I., Belloli, M., Ferrari, D., Fossati, F., and Giberti, H. (2014). Design of a 6-dof robotic platform for wind tunnel tests of floating wind turbines. *Energy Procedia*, 53:313–323.

Brandt, A. (2011). *Noise and vibration analysis: signal analysis and experimental procedures*. John Wiley & Sons.

Confalonieri, M., Ferrario, A., and Silvestri, M. (2018). Calibration of an on-board positioning correction system for micro-edm machines. In *EUSPEN Conference Proceedings - 18th International Conference and Exhibition*, pages 153–154.

Fu, Z.-F. and He, J. (2001). *Modal analysis*. Elsevier.

Giberti, H. and Ferrari, D. (2015). A novel hardware-in-the-loop device for floating offshore wind turbines and sailing boats. *Mechanism and Machine Theory*, 85(Supplement C):82 – 105.

Giberti, H., La Mura, F., Resmini, G., and Parmeggiani, M. (2018). Fully mechatronical design of an hil system for floating devices. *Robotics*, 7(3):39.

La Mura, F., Romanó, P., Fiore, E., and Giberti, H. (2018a). Workspace limiting strategy for 6 dof force controlled pkms manipulating high inertia objects. *Robotics*, 7(1):10.

La Mura, F., Todeschini, G., and Giberti, H. (2018b). High performance motion-planner architecture for hardware-in-the-loop system based on position-based-admittance-control. *Robotics*, 7(1):8.

Mejri, S., Gagnol, V., Le, T.-P., Sabourin, L., Ray, P., and Paultre, P. (2016). Dynamic characterization of machining robot and stability analysis. *The International Journal of Advanced Manufacturing Technology*, 82(1-4):351–359.

Palmieri, G., Martarelli, M., Palpacelli, M., and Carbonari, L. (2014). Configuration-dependent modal analysis of a cartesian parallel kinematics manipulator: numerical modeling and experimental validation. *Meccanica*, 49(4):961–972.

Silvestri, M., Pedrazzoli, P., Boër, C., and Rovere, D. (2011). Compensating high precision positioning machine tools by a self learning capable controller. In *Proceedings of the 11th international conference of the european society for precision engineering and nanotechnology*, pages 121–124.

Vu, V.-H., Liu, Z., Thomas, M., Li, W., and Hazel, B. (2016). Output-only identification of modal shape coupling in a flexible robot by vector autoregressive modeling. *Mechanism and Machine Theory*, 97:141–154.

Wiens, G. J. and Hardage, D. S. (2006). Structural dynamics and system identification of parallel kinematic machines. In *ASME 2006 International Design Engineering Technical Conferences and Computers and Information in Engineering Conference*, pages 749–758. American Society of Mechanical Engineers.